

# Structure model for the $\tau(\mu)$ phase in Al–Cr–Si alloys deduced from the $\lambda$ phase by the strong-reflections approach

H. Zhang,<sup>a</sup> Z.B. He,<sup>a</sup> P. Oleynikov,<sup>a</sup> X. D. Zou,<sup>a\*</sup> S. Hovmöller<sup>a</sup> and K. H. Kuo<sup>b</sup>

<sup>a</sup>Structural Chemistry, Stockholm University, SE-106 91 Stockholm, Sweden, and <sup>b</sup>Beijing Laboratory of Electron Microscopy, Institute of Physics, Chinese Academy of Sciences, PO Box 603, 100080 Beijing, People's Republic of China

Correspondence e-mail: zou@struc.su.se

Received 23 August 2005  
Accepted 1 November 2005

There are very obvious common features in the electron diffraction patterns of the  $\lambda$  and  $\tau(\mu)$  phases in the Al–Cr–Si system. The positions of the strong reflections and their intensity distributions are similar for the two structures. The relation of the reciprocal lattices of the  $\lambda$  and  $\tau(\mu)$  phases is studied. By applying the strong-reflections approach, the structure factors of  $\tau(\mu)$  are deduced from the corresponding structure factors of the known  $\lambda$  phase. Rules for selecting reflections for the strong-reflections approach are described. Similar to that of  $\lambda$ , the structure of  $\tau(\mu)$  contains six layers stacked along the  $c$  axis in each unit cell. There are 752 atoms in each unit cell, 53 of them are unique. The corresponding composition of the  $\tau(\mu)$  model is  $\text{Al}_{3.82-x}\text{CrSi}_x$ . Simulated electron diffraction patterns from the structure model are in good agreement with the experimental ones. The arrangement of interpenetrated icosahedral clusters in the  $\tau(\mu)$  phase is discussed.

## 1. Introduction

Since the discovery of the icosahedral quasicrystals in rapidly solidified Al–Mn alloys (Shechtman *et al.*, 1984), a large number of icosahedral and decagonal quasicrystals have been found in a variety of alloy systems. Great efforts have been made to solve the structures of the quasicrystals. One important approach is to start from the crystalline phases that are related to quasicrystals: quasicrystal approximants. Quasicrystals and their approximants are often found to coexist in alloys and they usually have well defined orientation relationships. Thus, determining the structures of quasicrystal approximants is very important. However, most approximants are hard to grow large enough for single-crystal X-ray diffraction as the structures are very complex and they are often disordered.

Electron crystallography is a powerful method for solving structures of crystals with sub-micrometer sizes, which are too small for X-ray crystallography. One of the main advantages of electron crystallography over X-rays is that the phases of crystallographic structure factors can be obtained directly from HREM images when the crystal is thin enough to almost satisfy the kinematic approximation. A rapidly increasing number of inorganic crystal structures, including minerals, oxides and metal clusters, have been solved by electron crystallography over the last 10 years (Weirich *et al.*, 1996). In most cases, the structures were solved from high-resolution images using Fourier-transform-based crystallographic image processing. Electron diffraction (ED) patterns have also been used alone for structure determination, where the structure-factor phases were determined by direct methods (Weirich *et al.*, 2000), by convergent-beam electron diffraction or by the

**Table 1**Crystallographic information for  $\beta$ ,  $\mu$ ,  $\lambda$  and  $\tau(\mu)$ .

Phases	Space group	$a$ (Å)	$c$ (Å)
$\beta$	$P6_3/mmc$	7.513	7.745
$\mu$	$P6_3/mmc$	19.98	24.673
$\lambda$	$P6_3/m$	28.382	12.389
$\tau(\mu)$	$P6_3/mmc$	32.3	12.4

Patterson method from precession electron-diffraction data (Gjønnnes *et al.*, 1998).

Recently, the three-dimensional structure of a huge quasicrystal approximant  $\nu$ -AlCrFe (space group  $P6_3/m$ ,  $a = 40.687$  and  $c = 12.546$  Å) was solved by three-dimensional electron crystallography. The structure was determined from high-resolution electron microscopy (HREM) images and electron diffraction patterns from 13 different zone axes (Zou *et al.*, 2003). The structure was similar to that obtained from single-crystal X-ray diffraction (Mo *et al.*, 2000). The  $\nu$ -AlCrFe phase is related to several other hexagonal phases, for example, the  $\kappa$  (Li *et al.*, 1997; Marsh, 1998;  $a = 17.674$  and  $c = 12.516$  Å) and  $\lambda$  (Kreiner & Franzen, 1997;  $a = 28.382$  and  $c = 12.389$  Å) phases; all of them have the same space group  $P6_3/m$ . By analysing the relationship of the reciprocal lattices and the structure-factor phases and amplitudes of this series of approximants we found that the strong reflections that are close to each other in reciprocal space have similar structure-factor amplitudes and identical structure-factor phases for all these approximants (Zhang *et al.*, 2006). This important observation led us to a new approach for deducing or solving unknown structures, especially quasicrystal approximants, from known related structures. We call this new approach 'the strong-reflections approach' (Christensen *et al.*, 2004). The structure-factor phases of the strong reflections of an unknown structure are deduced from those of a known related structure, while the structure-factor amplitudes of the unknown structure can be obtained either experimentally, by X-ray or electron diffraction, or even deduced from those of the known related structure. Atomic positions are obtained directly from the three-dimensional map calculated from the structure-factor amplitudes obtained and the phases of the strong reflections. The strong-reflections approach is also based on two other important facts: for *solving* structures, only the strongest reflections are needed and their structure-factor phases must be correct. When the strongest reflections with correct phases are included in the calculation of the three-dimensional map, the structure model obtained is correct to the extent that 90–100% of the heaviest atoms are found within  $\sim 0.2$  Å from their correct positions (Weirich *et al.*, 1996). Such a model can be further refined against accurate experimental X-ray or electron diffraction data when they are available.

Sometimes one or more of the unit-cell dimensions of different approximants within the same series are related by the golden number  $\tau$  as 1:  $\tau$ :  $\tau^2$ :  $\tau^3$  *etc.* The strong-reflections approach was applied to a series of approximants in the Al–Co

system. From  $m$ -Al<sub>13</sub>Co<sub>4</sub> ( $C2/m$ ,  $a = 15.173$ ,  $b = 8.109$ ,  $c = 12.349$  Å and  $\beta = 107.84^\circ$ ), the structure of  $\tau^2$ -Al<sub>13</sub>Co<sub>4</sub> ( $P2/m$ ,  $a = 39.863$ ,  $b = 8.139$ ,  $c = 32.208$  Å and  $\beta = 107.96^\circ$ ) was solved (Christensen *et al.*, 2004).

Recently, more extensive studies of the crystalline and quasicrystalline phases in Al rich Al–Cr–Si alloys with a Si content less than 10 at% have been carried out (He & Kuo, 2004). Four hexagonal quasicrystal approximants,  $\beta$ ,  $\mu$ ,  $\lambda$  and  $\tau(\mu)$ , have been found to coexist with a decagonal quasicrystal in these alloys. Their space groups and unit-cell parameters are listed in Table 1.<sup>1</sup> Three of them, the  $\beta$ ,  $\mu$  and  $\lambda$  phases, have previously been found in Al–Mn systems. Their structures were determined by single-crystal X-ray diffraction (Taylor, 1959; Robinson, 1952; Shoemaker *et al.*, 1989; Kreiner & Franzen, 1997). The hexagonal  $\tau(\mu)$  phase is a new phase in these alloys. It has the same space group ( $P6_3/mmc$ ) as the  $\beta$  and  $\mu$  phases; the  $a$  parameter of  $\tau(\mu)$  is  $\tau$  times larger than that of the  $\mu$  phase, but the  $c$  parameter is only half that of the  $\mu$  phase. By studying the relationship of the unit cell between  $\tau(\mu)$  and  $\mu$ -Al<sub>4</sub>Mn phases and considering the arrangement of chains of interpenetrating icosahedra, a structure model of  $\tau(\mu)$  was proposed from the  $\mu$  phase (He & Kuo, 2004). This real-space approach has also been used to obtain structure models of several other quasicrystal approximants (Mo *et al.*, 1998).

In the present paper, we are applying a different approach (the strong-reflection approach) to deduce the structure of the  $\tau(\mu)$  phase. This is a reciprocal-space approach. We also propose the rules for how to select the strong reflections.

## 2. Common features of the $\lambda$ and $\tau(\mu)$ phases

We will here deduce  $\tau(\mu)$  not from  $\mu$  but from the  $\lambda$  phase since both have  $c \simeq 12.4$  Å. Thus,  $\lambda$  and  $\tau(\mu)$  are both made up of six layers stacked along the  $c$  axis. Although the symmetry of  $\tau(\mu)$  is higher than that of  $\lambda$ , their diffraction patterns are quite similar, as shown in Fig. 1. Interestingly, the intensity distribution of the strong reflections in the  $\lambda$  phase closely follows a higher symmetry than what is required for the space group:  $6/mmm$  rather than  $6/m$ , even though the reflections are misplaced slightly from the  $6/mmm$  symmetry (see Fig. 1). The corresponding strongest spots can be easily identified, for example (1350) in  $\lambda$  corresponds to (13,00) in  $\tau(\mu)$ ; (11,20) in  $\lambda$  to (880) in  $\tau(\mu)$ ; (580) in  $\lambda$  to (013,0) in  $\tau(\mu)$ . This indicates that the strong reflections of the  $\lambda$  phase obey the same symmetry rules as those for  $\tau(\mu)$ . Accordingly, it should be possible to solve the structure of the  $\tau(\mu)$  phase from those strong reflections, as is attempted in this paper.

## 3. Relating the reciprocal lattice of $\lambda$ to that of $\tau(\mu)$

All the strong reflections in the reciprocal lattices of the  $\lambda$  and  $\tau(\mu)$  phases coincide, which means that the ( $hkl$ ) indices of the

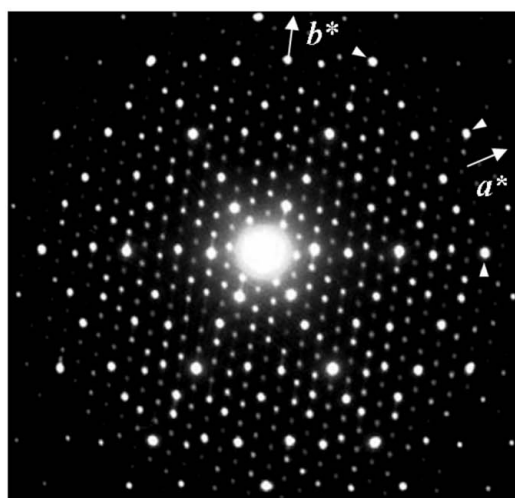
<sup>1</sup> Supplementary data for this paper are available from the IUCr electronic archives (Reference: DR5007). Services for accessing these data are described at the back of the journal.

strong reflections in these two approximants are related, by the matrix  $A$

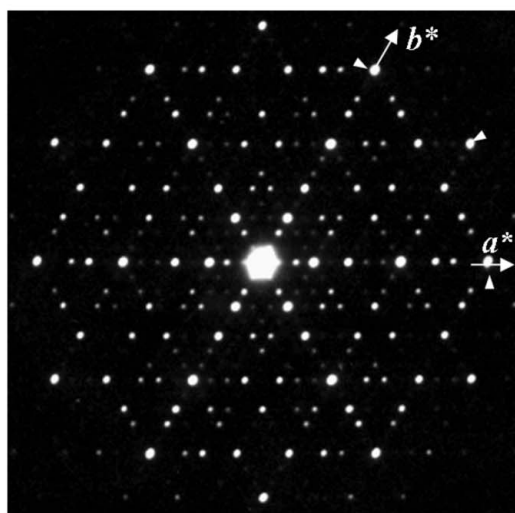
$$(hkl)_{\tau(\mu)} = (hkl)_\lambda \cdot A. \tag{1}$$

Matrix  $A$  can be deduced from the indices of the corresponding strong reflections, for example,  $(006)_\lambda \simeq (006)_{\tau(\mu)}$ ,  $(13, \bar{5}0)_\lambda \simeq (13, 00)_{\tau(\mu)}$  and  $(11, 20)_\lambda \simeq (880)_{\tau(\mu)}$ , using a curve fitting program, such as *LAB Fit* (Silva & Silva, 2005).  $A$  becomes

$$A = \begin{pmatrix} \tau/2 & 1/2 & 0 \\ -1/2 & \tau^2/2 & 0 \\ 0 & 0 & 1 \end{pmatrix}. \tag{2}$$



(a)



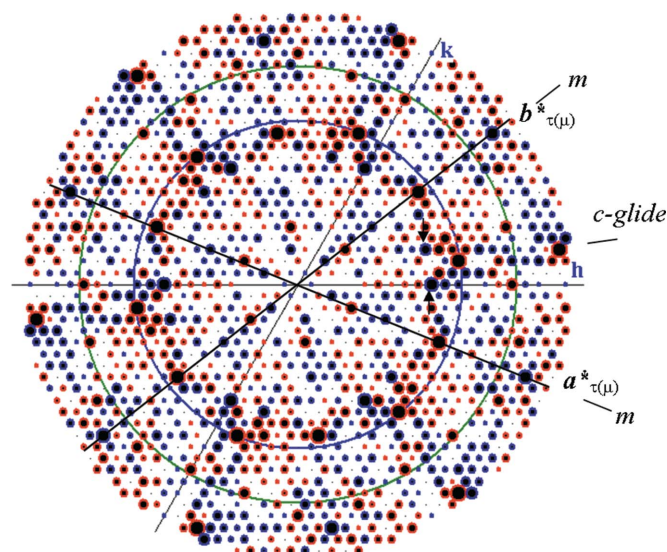
(b)

**Figure 1**

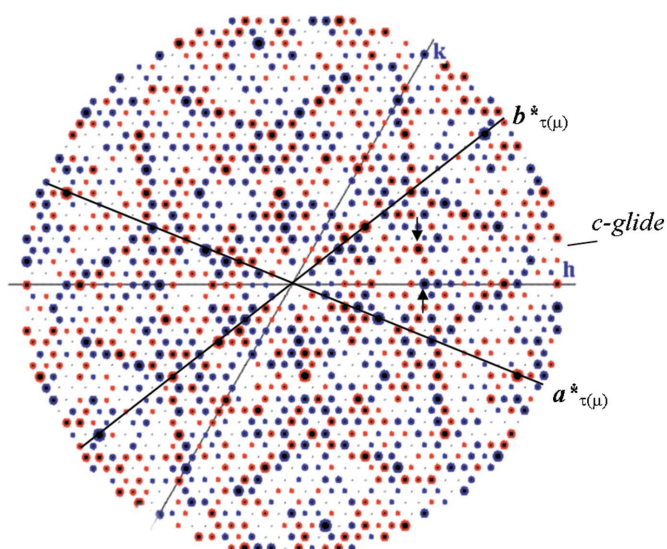
Electron diffraction patterns from (a) the  $\lambda$  and (b) the  $\tau(\mu)$  approximants taken at 100 kV along the  $c$  axis, both are on the same scale and with similar orientation. The corresponding strongest diffraction spots in the two approximants are marked by arrows. The diffraction pattern of  $\lambda$  in (a) shows  $p6$  symmetry, while that of  $\tau(\mu)$  in (b) shows  $p6m$  symmetry. Note, however, that the strongest diffraction spots in  $\lambda$  (a) have approximate  $p6m$  symmetry.

Correct crystallographic structure-factor phases are more important than accurate amplitudes for solving crystal structures. The  $hk0$  and  $hk1$  reciprocal layers of calculated structure factors of  $\lambda$  are shown in Fig. 2. Some reflections are very much stronger than the average reflections. This is a typical feature of quasicrystals and approximants. When a density map is calculated, the contributions from these few strong reflections will dominate the density map. Thus, for solving the structure of  $\tau(\mu)$  from  $\lambda$  we must pay most attention to these strong reflections.

The space group of  $\lambda$  ( $P6_3/m$ ) is lower than the space group of  $\tau(\mu)$ ,  $P6_3/mmc$ . Both space groups have one mirror plane perpendicular to the  $6_3$  screw axis ( $c$  axis). In  $P6_3/mmc$ , there is



(a)



(b)

**Figure 2**

Calculated structure factors of  $\lambda$ ; (a)  $hk0$  and (b)  $hk1$  layers. The spot sizes correspond to the relative structure-factor amplitudes. Reflections with phase  $0^\circ$  are red, while those with phase  $180^\circ$  are blue. The large blue and green circles indicate 2.0 and 1.5 Å resolution. Two approximate mirror planes  $m$  and one approximate glide plane  $c$  in  $\tau(\mu)$  are indicated.

an additional  $c$  glide plane normal to the  $[210]$  direction, which generates another mirror plane normal to the  $a$  axis. As a consequence, in reciprocal space for  $\tau(\mu)$  there are an additional  $c$  glide in the plane of  $\mathbf{c}^*_{\tau(\mu)}$  and the diagonal of  $\mathbf{a}^*_{\tau(\mu)}$  and  $\mathbf{b}^*_{\tau(\mu)}$ , and a mirror plane in the  $\mathbf{c}^*_{\tau(\mu)}$  plane, which are not present in  $\lambda$  (see Fig. 2). Also the phase relations are different in  $P6_3/m$  and  $P6_3/mmc$ . Reflections with  $l = 2n$ , such as  $(10,00)$  and  $(830)$  (indicated by arrows in Fig. 2*a*), are crystallographically independent in  $P6_3/m$  ( $\lambda$ ), but the corresponding reflections in  $\tau(\mu)$  (850) and (580) are symmetry-related in  $P6_3/mmc$  and have the same phase values. Similarly, independent reflections with  $l = 2n + 1$ , such as  $(10,01)$  and  $(831)$  (indicated by arrows in Fig. 2*b*), which are independent in  $\lambda$ , correspond to symmetry-related reflections in  $\tau(\mu)$ , (851) and (581). In the  $\lambda$  phase, being  $P6_3/m$ , the reflections  $(10,01)$  and  $(831)$  are crystallographically independent and thus their phases may be the same or differ by  $180^\circ$ . However, in  $\tau(\mu)$ , being  $P6_3/mmc$ , these reflections correspond to (851) and (581) and their phases must differ by  $180^\circ$  (*i.e.* one of them is  $0^\circ$  and the other is  $180^\circ$ ) because of the  $c$  glide plane.

The corresponding reflections from two related structures have the same phase values if they have similar intensity distributions in reciprocal space (Christensen *et al.*, 2004; Zhang *et al.*, 2005). The strong spots in  $\tau(\mu)$  and  $\lambda$  have very similar intensity distributions in reciprocal space. Thus, we can

assume that the strong reflections in  $\tau(\mu)$  will have the same amplitude and phase values as their counterparts in  $\lambda$ . In order to obtain the structure factors of  $\tau(\mu)$ , we adapted the phases and amplitudes from the corresponding reflections in  $\lambda$ , using the following procedure.

The structure factors of  $\lambda$  were calculated to  $1.2 \text{ \AA}$  resolution with the program *LAZY* (Yvon *et al.*, 1977) from the atomic coordinates of the  $\lambda$  phase solved by X-ray diffraction (Kreiner & Franzen, 1997). We expect that we can have enough accuracy for atomic positions of the structure with  $1.2 \text{ \AA}$  reciprocal space resolution. In total, there are 1881 unique reflections inside a resolution of  $1.2 \text{ \AA}$ . The indices of the corresponding reflections in  $\tau(\mu)$  were calculated from the reflections in  $\lambda$  using (1). The 50 strongest among these 1881 reflections are listed in Table 2, with structure-factor amplitudes and phases for  $\lambda$ . The calculated  $hkl$  indices for  $\tau(\mu)$  are also listed. Integer indices for  $\tau(\mu)$  were obtained by rounding the decimal numbers to the nearest integers. The deviations between unrounded and rounded indices of  $\tau(\mu)$  are the differences between  $\tau(\mu)$  and  $\lambda$  in reciprocal space (see the last column of Table 2). The deviations for the strongest reflections are very small ( $< 0.004 \text{ \AA}^{-1}$ ), much smaller than the reciprocal lattice parameters of  $\tau(\mu)$  ( $a^*_{\tau(\mu)} = 0.0357$  and  $c^*_{\tau(\mu)} = 0.0931 \text{ \AA}^{-1}$ ).

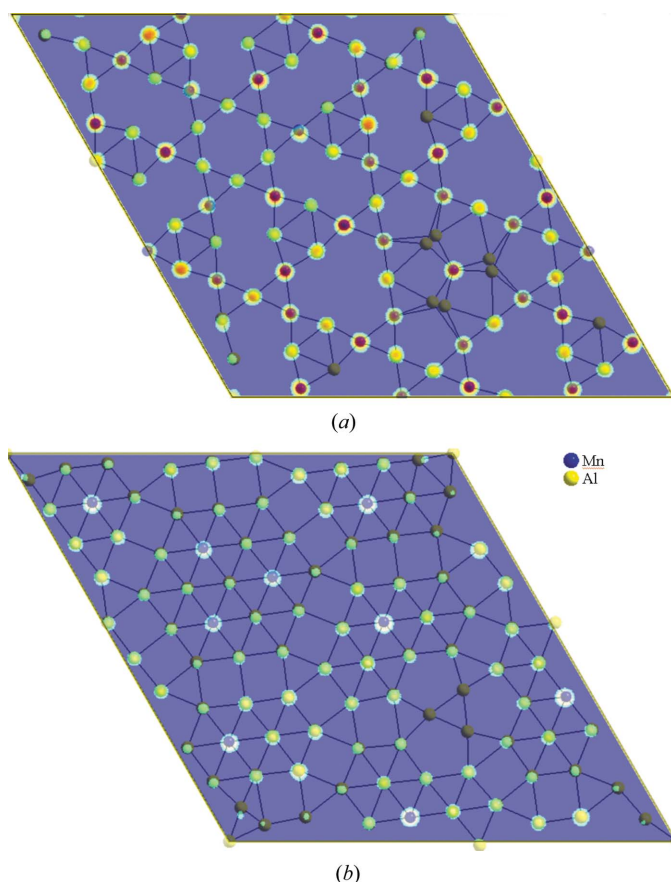


**Figure 3**  
The three-dimensional density map of  $\lambda$  obtained from the 308 unique strong reflections, with the structure model superimposed. The flat layer at (a)  $z = 1/4$  and the puckered layer at (b)  $z \approx 0.1$ .

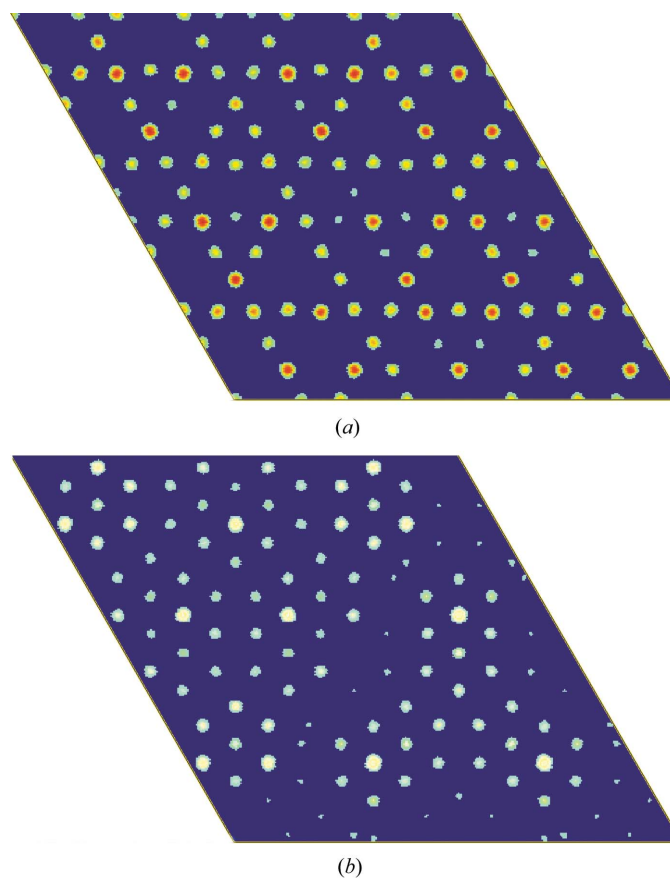


**Figure 4**  
The three-dimensional density map of  $\tau(\mu)$  obtained from the 218 unique strong reflections deduced from  $\lambda$ . (a) The flat layer ( $z = 1/4$ ) and (b) the puckered layer ( $z \approx 0.1$ ).

**Table 2**

The 50 largest structure factors in  $\lambda$  and the corresponding indices of  $\tau(\mu)$  deduced from  $\lambda$  with 2 decimals and as the nearest integers.

Dev. is the deviation between the corresponding reflections of  $\lambda$  and  $\tau(\mu)$  in reciprocal space.

No.	Structure factors of $\lambda$				Phases	Indices of $\tau(\mu)$ with 2 decimals			Indices of $\tau(\mu)$ with integers			Dev. ( $\times 10^2 \text{ \AA}^{-1}$ )
	<i>h</i>	<i>k</i>	<i>l</i>	Amplitudes		<i>h</i>	<i>k</i>	<i>l</i>	<i>h</i>	<i>k</i>	<i>l</i>	
1	0	0	6	3522	180	0.00	0.00	6	0	0	6	0.00
2	18	3	0	3089	0	13.07	12.92	0	13	13	0	0.28
3	0	0	10	3013	180	0.00	0.00	10	0	0	10	0.00
4	5	8	8	2864	0	0.07	12.96	8	0	13	8	0.22
5	5	8	2	2750	180	0.07	12.96	2	0	13	2	0.22
6	8	13	3	2479	180	0.01	20.99	3	0	21	3	0.04
7	11	2	0	2368	0	7.91	8.11	0	8	8	0	0.37
8	3	5	5	2287	0	-0.06	8.04	5	0	8	5	0.18
9	10	0	3	2171	180	8.09	5.00	3	8	5	3	0.33
10	8	3	3	2127	0	4.98	7.92	3	5	8	3	0.32
11	5	8	0	1943	0	0.07	12.96	0	0	13	0	0.22
12	13	5	5	1630	180	8.03	13.03	5	8	13	5	0.21
13	16	0	5	1558	0	12.95	8.00	5	13	8	5	0.19
14	2	3	5	1269	180	0.13	4.92	5	0	5	5	0.40
15	11	2	6	1068	180	7.91	8.11	6	8	8	6	0.37
16	8	13	0	1064	180	0.01	20.99	0	0	21	0	0.04
17	3	5	4	952	0	-0.06	8.04	4	0	8	4	0.18
18	0	0	8	937	0	0.00	0.00	8	0	0	8	0.00
19	0	0	2	933	180	0.00	0.00	2	0	0	2	0.00
20	5	8	4	927	0	0.07	12.96	4	0	13	4	0.22
21	10	0	0	917	180	8.09	5.00	0	8	5	0	0.33
22	13	5	6	898	180	8.03	13.03	6	8	13	6	0.21
23	16	0	6	869	180	12.95	8.00	6	13	8	6	0.19
24	6	10	5	822	180	-0.12	16.07	5	0	16	5	0.36
25	3	15	2	784	180	-5.03	21.11	2	-5	21	2	0.34
26	8	3	0	761	180	4.98	7.92	0	5	8	0	0.32
27	11	8	2	754	180	4.92	15.96	2	5	16	2	0.38
28	0	0	4	749	0	0.00	0.00	4	0	0	4	0.00
29	2	3	6	715	180	0.13	4.92	6	0	5	6	0.40
30	9	3	0	711	0	5.79	8.42	0	6	8	0	1.30
31	8	13	2	670	180	0.01	20.99	2	0	21	2	0.04
32	8	13	4	639	0	0.01	20.99	4	0	21	4	0.04
33	3	5	9	626	180	-0.06	8.04	9	0	8	9	0.18
34	9	1	3	625	0	6.79	5.81	3	7	6	3	1.26
35	3	5	1	598	0	-0.06	8.04	1	0	8	1	0.18
36	10	0	9	585	0	8.09	5.00	9	8	5	9	0.33
37	2	4	5	583	0	-0.37	6.23	5	0	6	5	1.15
38	9	4	0	577	0	5.29	9.73	0	5	10	0	1.01
39	7	11	3	573	0	0.20	17.88	3	0	18	3	0.61
40	8	3	9	566	180	4.98	7.92	9	5	8	9	0.32
41	8	13	1	564	180	0.01	20.99	1	0	21	1	0.04
42	10	6	5	557	0	5.11	12.84	5	5	13	5	0.50
43	13	5	3	555	0	8.03	13.03	3	8	13	3	0.21
44	10	0	7	546	180	8.09	5.00	7	8	5	7	0.33
45	18	4	0	543	180	12.58	14.23	0	13	14	0	1.31
46	5	8	6	540	180	0.07	12.96	6	0	13	6	0.22
47	10	0	2	536	180	8.09	5.00	2	8	5	2	0.33
48	16	0	3	529	180	12.95	8.00	3	13	8	3	0.19
49	8	3	7	528	0	4.98	7.92	7	5	8	7	0.32
50	9	2	3	526	180	6.29	7.11	3	6	7	3	1.28

The structure-factor phases of  $\tau(\mu)$  derived from  $\lambda$  as described above were checked layer by layer (from  $hk0$  to  $hk10$ ). For all the strongest reflections, the phases of symmetry-related reflections fulfil the phase-restriction rules of  $P6_3/mmc$  [ $\tau(\mu)$  symmetry];  $\text{Phase}(khl) = \text{Phase}(hkl) + l \cdot 180^\circ$ . The strongest structure-factor amplitude  $|F_{hkl}|$  in  $\lambda$  is 3522 for (006) (Table 2). For the weakest reflections ( $|F_{hkl}| < 100$ ), many reflection pairs do not obey the phase relation rules described above. Thus, the phases of the strongest reflections of  $\tau(\mu)$  can be derived from the phases of the

corresponding reflections in the  $\lambda$  phase, but this method cannot be used for phasing the weak reflections. Therefore, we only use the 645 strong reflections with  $|F_{hkl}| \geq 100$  of the total 1881 unique reflections for calculating the density map of  $\tau(\mu)$ , summing up to 75% of the total amplitude.

In the next step, reflections of  $\lambda$  falling far from the positions of  $\tau(\mu)$  were deleted, since the more a reflection pair of two structures deviates from each other in reciprocal space, the less their phases will be related. We found that all reflections of  $\lambda$  (308 unique) with the deviation  $\leq 0.0103 \text{ \AA}^{-1}$  [29%

**Table 3**

Atomic coordinates of  $\lambda$  determined from the density map calculated from only 308 strong unique reflections compared with those determined by X-ray diffraction (Kreiner & Franzen, 1997).

The uncertainty of the coordinates for the present study is at the third decimal ( $ca \pm 0.003$ ), much higher than those by X-ray diffraction (at the fourth decimal). Deviations between the two sets of atomic coordinates are given; the average deviation is 0.20 Å. The peaks are numbered with descending heights.

Atomic coordinates from X-ray diffraction				Atomic coordinates from 308 reflections				Deviation (Å)
Atom	<i>x</i>	<i>y</i>	<i>z</i>	Peak	<i>x</i>	<i>y</i>	<i>z</i>	
Mn66	0.4347	0.0619	0.0743	1	0.435	0.059	0.073	0.10
Mn32	0.4774	0.4502	0.2500	2	0.477	0.449	0.250	0.03
Mn27	0.2854	0.3315	0.2500	3	0.282	0.328	0.250	0.11
Mn28	0.3599	0.5270	0.2500	4	0.356	0.523	0.250	0.13
Mn24	0.1661	0.0220	0.2500	5	0.164	0.020	0.250	0.07
Mn29	0.3620	0.1455	0.2500	6	0.362	0.141	0.250	0.15
Mn64	0.1274	0.2571	0.0744	7	0.127	0.251	0.071	0.20
Al4	0.0517	0.3364	0.2500	8	0.051	0.333	0.250	0.10
Mn1	0.6667	0.3333	0.2500	9	0.667	0.333	0.250	0.02
Mn26	0.2418	0.2192	0.2500	10	0.240	0.218	0.250	0.05
Al47	0.2465	0.1834	0.0695	11	0.246	0.178	0.071	0.17
Mn23	0.1188	0.3079	0.2500	12	0.116	0.302	0.250	0.17
Mn31	0.4724	0.2119	0.2500	13	0.472	0.209	0.250	0.09
Al9	0.1823	0.2661	0.2500	14	0.175	0.260	0.250	0.22
Mn33	0.5897	0.1364	0.2500	15	0.548	0.407	0.250	0.13
Mn30	0.3840	0.0019	0.2500	16	0.384	0.000	0.250	0.06
Mn65	0.2445	0.5632	0.0710	17	0.246	0.562	0.071	0.08
Al17	0.4223	0.1055	0.2500	18	0.427	0.110	0.250	0.15
Al16	0.3815	0.3796	0.2500	19	0.381	0.381	0.250	0.06
Al15	0.3102	0.1918	0.2500	20	0.308	0.186	0.250	0.16
Al20	0.5079	0.3105	0.2500	21	0.503	0.308	0.250	0.14
Mn25	0.1992	0.5012	0.2500	22	0.192	0.500	0.250	0.22
Al49	0.3172	0.3719	0.0677	23	0.319	0.370	0.071	0.11
Al51	0.3332	0.2858	0.1341	24	0.333	0.282	0.135	0.12
Al19	0.4872	0.0667	0.2500	25	0.492	0.068	0.250	0.14
Al45	0.2134	0.3552	0.1349	26	0.215	0.353	0.135	0.11
Al46	0.2320	0.2714	0.0629	27	0.232	0.268	0.063	0.11
Al10	0.1952	0.1213	0.2500	28	0.192	0.116	0.250	0.15
Al61	0.5370	0.0767	0.0652	29	0.540	0.458	0.062	0.17
Al7	0.0957	0.4529	0.2500	30	0.093	0.446	0.250	0.19
Al34	0.0231	0.4721	0.1348	31	0.023	0.469	0.135	0.10
Al2	0.0000	0.0000	0.1378	32	0.000	0.000	0.250	1.39
Al37	0.0405	0.3884	0.0550	33	0.040	0.384	0.058	0.14
Al58	0.4506	0.3564	0.1363	34	0.452	0.356	0.133	0.07
Al62	0.5551	0.3780	0.0680	35	0.554	0.370	0.070	0.24
Al6	0.0785	0.2050	0.2500	36	0.074	0.192	0.250	0.37
Al56	0.4207	0.1494	0.0624	37	0.421	0.150	0.060	0.03
Al41	0.1435	0.1705	0.1363	38	0.144	0.167	0.135	0.12
Al11	0.2328	0.6036	0.2500	39	0.237	0.604	0.250	0.13
Al57	0.4365	0.4460	0.0692	40	0.435	0.444	0.071	0.06
Al14	0.3060	0.4257	0.2500	41	0.308	0.424	0.250	0.10
Al52	0.3344	0.0463	0.1356	42	0.336	0.045	0.135	0.08
Al60	0.5188	0.1606	0.1372	43	0.523	0.161	0.135	0.13
Al13	0.2950	0.5668	0.2500	44	0.294	0.565	0.250	0.05
Al48	0.2594	0.4759	0.1358	45	0.257	0.472	0.135	0.11
Al42	0.1440	0.5474	0.1350	46	0.144	0.545	0.135	0.08
Al54	0.3636	0.4906	0.0682	47	0.364	0.486	0.071	0.16
Al18	0.4289	0.5012	0.2500	48	0.429	0.500	0.250	0.04
Al55	0.4082	0.2398	0.1367	49	0.407	0.237	0.131	0.11
Al59	0.5072	0.2497	0.0681	50	0.508	0.249	0.068	0.04
Al53	0.3479	0.5802	0.0570	51	0.348	0.576	0.062	0.15
Al8	0.1646	0.4068	0.2500	52	0.164	0.401	0.250	0.18
Al40	0.1121	0.3430	0.0571	53	0.113	0.342	0.057	0.05
Al3	0.3333	0.6667	0.1188	54	0.333	0.667	0.131	0.15
Al35	0.0273	0.2416	0.1361	55	0.025	0.237	0.136	0.13
Al36	0.0406	0.1543	0.0578	56	0.040	0.150	0.058	0.13
Al50	0.3188	0.1362	0.0692	57	0.319	0.133	0.070	0.11
Al43	0.1570	0.4616	0.0564	58	0.155	0.455	0.057	0.19
Al5	0.0531	0.1007	0.2500	59	0.048	0.099	0.250	0.15
Al38	0.0694	0.0871	0.0496	60	0.056	0.065	0.067	0.66
Al44	0.2011	0.0630	0.0677	61	0.203	0.062	0.073	0.11
Al39	0.0999	0.0424	0.1411	62	0.099	0.045	0.131	0.16
Al12	0.2665	0.0728	0.2500	–	–	–	–	–
Al21	0.5773	0.2487	0.2500	–	–	–	–	–
Al22	0.5991	0.2382	0.2500	–	–	–	–	–
Al63	0.6099	0.3269	0.1000	–	–	–	–	–

of  $a_{\tau(\mu)}^*$ ] obey the higher  $6/mmm$  symmetry of  $\tau(\mu)$ . The amplitudes of these 308 reflections cover 50% of the total amplitudes from 1881 reflections. We expect that if we use the phases and amplitudes of these 308 reflections in  $\lambda$  and transform them to the structure factors of  $\tau(\mu)$ , a reasonable structure model of  $\tau(\mu)$  may be obtained.

#### 4. The $\lambda$ structure deduced from 308 strong reflections

To see if the 308 strong unique reflections are sufficient to obtain a good enough density map, we first checked it on the  $\lambda$  structure. A three-dimensional density map was calculated by the three-dimensional inverse Fourier transformation of the 308 strong structure factors for  $\lambda$ , using the *eMap* program (Oleynikov *et al.*, 2005). The three-dimensional map was sampled with 0.04 Å per pixel, sufficient to keep a 0.2 Å accuracy of atomic positions. The three-dimensional density map was examined section by section perpendicular to the *c* axis. There are six layers stacked along the *c* axis in each unit cell, only two of them are unique; one flat layer and one puckered layer. The flat (*F*) and puckered layers (*P*) are stacked in a sequence of  $PF P^m(PFP^m)'$ , where  $P^m$  is related to *P* via a mirror reflection on the flat layer, and the  $(PFP^m)'$  block is related to the  $(PF P^m)$  block by a  $6_3$  operation along the *c* axis. The flat and puckered layers of the density map calculated using the 308 strong unique reflections are compared with the structure model determined by X-ray crystallography (Kreiner & Franzen, 1997; see also Fig. 3). The density maps are clear, with round and well resolved peaks; 62 of the 66 unique atoms in  $\lambda$  were found. The atomic coordinates obtained from the density map are quite similar to those determined by X-ray diffraction (see Table 3); 59 unique atoms (89%) deviate on average by 0.12 Å (maximum 0.24 Å); two by 0.37 (Al6) and 0.66 Å (Al38), respectively, and one on the  $6_3$  screw axis (Al2) is severely misplaced by 1.39 Å along the *c* axis. Three of the four atoms that are missing are near one of the threefold axes (see Fig. 3).

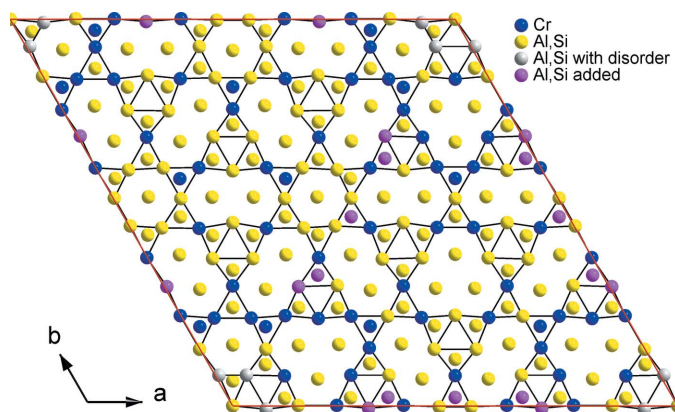


**Figure 5**  
The final structure model of  $\tau(\mu)$  deduced from  $\lambda$  using the strong-reflections approach (only those atoms within  $z = 0-0.5$  are shown). Atoms on the flat layer are connected by lines and those on the puckered layers are left unconnected.

All the 15 unique Mn atoms are found with 0.11 Å deviations on average from the X-ray model and they are among the highest 22 peaks. The first Al peak is the eighth strongest (Al4). Although the heavy atoms are among the strongest peaks, the peak heights may not always agree with the atomic numbers when only a limited number of strong reflections is included. In conclusion, it is possible to solve a structure with 90% or more of the atoms being accurately determined, from a limited number of strong reflections. However, we need to use both the peak heights and chemical knowledge to assign the atom types. In the following we will use the 308 unique reflections of  $\lambda$  to derive a structure model of the  $\tau(\mu)$  phase.

#### 5. The $\tau(\mu)$ structure deduced from the 218 strong unique reflections

Since the symmetry of  $\tau(\mu)$  is higher than that of  $\lambda$ , the 308 unique reflections of  $\lambda$  correspond to only 218 unique reflections for  $\tau(\mu)$  after merging according to the space group  $P6_3/mmc$ . The indices of the reflections for  $\tau(\mu)$  are derived from  $\lambda$  using (1). The structure-factor amplitudes and phases of the reflections in  $\tau(\mu)$  are set equal to their counterparts in  $\lambda$ . The structure factors of these 218 unique reflections were expanded to a total of 1892 structure factors of  $\tau(\mu)$  and a three-dimensional density map was calculated in a similar way as described for the  $\lambda$  phase. Similar to the  $\lambda$  structure, there are six layers stacked along the *c* axis in each unit cell, two of them are unique: a flat layer ( $z = 1/4$ ) and a puckered layer ( $z \simeq 0.10$ ), as shown in Fig. 4.

The three-dimensional density maps show round and well resolved peaks. Most peaks have reasonable distances from each other (2.2–2.5 Å). There were 51 peaks found in the asymmetric unit of the three-dimensional density map and their coordinates were determined by *eMap* (Table 4). The assignment of different atoms to the peaks was carried out by both considering the peak heights and taking into account the chemical knowledge, as suggested in §4. The first 13 highest peaks and peak 18 were assigned to be Cr atoms. All the other peaks were assigned to be Al or Si (Al and Si are too similar to be distinguished). Peak 46 was removed because it is too close to the neighbouring atoms. Peak 51 generates six atoms that were too close to each other. We consider that they are disordered and only three of them can be occupied simultaneously, and the corresponding occupancy is thus 0.5. Three atomic positions (atoms 52–54) were added for completing the characteristic icosahedra. The final atomic coordinates for  $\tau(\mu)$  are listed in Table 4. There are 752 atoms in each unit cell, 53 of them are unique. The corresponding composition of the  $\tau(\mu)$  model is  $Al_{3.82-x}CrSi_x$ . It should be mentioned that the structure model is only preliminary and may be not completely correct. There may be problems with the assignment of atom type at some positions and with the identification of some Al/Si positions. We have not yet managed to produce crystals of the  $\tau(\mu)$  phase good enough for single-crystal X-ray diffraction and so do not have a complete data set that would allow us to refine the structure model.

**Table 4**

Atomic positions of the final structure model for  $\tau(\mu)$  obtained from the density map using the 218 unique reflections.

The atoms are numbered with descending heights. Atom 51 has an occupancy of 0.5; atoms 52–54 are added. The standard deviations are estimated to be 0.003 for all coordinates.

Atom	<i>x</i>	<i>y</i>	<i>z</i>
Cr1	0.412	0.206	0.072
Cr2	0.305	0.459	0.250
Cr3	0.155	0.310	0.250
Cr4	0.155	0.078	0.250
Cr5	0.413	0.587	0.072
Cr6	0.305	0.226	0.250
Cr7	0.538	0.310	0.250
Cr8	0.539	0.461	0.250
Cr9	0.176	0.205	0.072
Cr10	0.155	0.227	0.250
Cr11	0.384	0.616	0.250
Cr12	0.234	0.233	0.250
Cr13	0.382	0.232	0.250
Al14	0.617	0.383	0.250
Al15	0.176	0.351	0.069
Al16	0.464	0.232	0.250
Al17	0.225	0.301	0.135
Cr18	0.385	0.383	0.250
Al19	0.391	0.311	0.250
Al20	0.304	0.608	0.250
Al21	0.236	0.381	0.250
Al22	0.390	0.460	0.250
Al23	0.510	0.255	0.063
Al24	0.608	0.304	0.135
Al25	0.412	0.442	0.069
Al26	0.385	0.536	0.250
Al27	0.127	0.254	0.063
Al28	0.148	0.146	0.250
Al29	0.000	0.000	0.250
Al30	0.362	0.253	0.059
Al31	0.459	0.299	0.135
Al32	0.557	0.350	0.069
Al33	0.316	0.540	0.135
Al34	0.079	0.158	0.135
Al35	0.315	0.391	0.135
Al36	0.318	0.159	0.135
Al37	0.364	0.636	0.056
Al38	0.362	0.489	0.063
Al39	0.266	0.440	0.072
Al40	0.237	0.474	0.250
Al41	0.460	0.540	0.132
Al42	0.526	0.380	0.250
Al43	0.275	0.254	0.056
Al44	0.560	0.440	0.076
Al45	0.463	0.465	0.250
Al47	0.226	0.156	0.135
Al48	0.460	0.391	0.135
Al49	0.127	0.107	0.059
Al50	0.032	0.065	0.066
Al51	0.071	0.079	0.250
Al52	0.302	0.308	0.250
Al53	0.511	0.489	0.069
Al54	0.360	0.338	0.069

Two flat layers (*F*) and four puckered layers (*P*) are stacked along the *c* axis in each unit cell, in a sequence of  $PFP^m(PFP^m)'$ , where  $P^m$  is related to *P* via a mirror reflection on the flat layer and the  $(PFP^m)'$  block is related to the  $(PFP^m)$  block by a  $6_3$  operation along the *c* axis. The  $(PFP^m)$  block ( $z = 0-0.5$ ) of the final structure model for  $\tau(\mu)$  is shown in Fig. 5.

The structure of  $\tau(\mu)$  can also be represented as chains of interpenetrating icosahedra (Fig. 6*a*). There are five such chains running along the  $\langle 100 \rangle$  directions in each unit cell, with the sequences  $2 + 4 + 2$ ,  $3 + 4 + 3$ ,  $4 + 4 + 2$ ,  $4 + 4 + 2$  and  $4 + 3 + 3$ , respectively. The structure model of the  $\tau(\mu)$  phase presented here resembles that proposed by He & Kuo (2004), constructed by model-building based on the  $\mu$  phase. Most of the atoms superpose if the two models are rotated by  $30^\circ$  and shifted by nearly  $(\frac{1}{2} \frac{1}{2} 0)$ . Compared with the structure of  $\lambda$ , both can be described by chains of interpenetrating icosahedra. However, in  $\lambda$ , the chains are rotated by  $27^\circ$  with respect to the  $\langle 100 \rangle$  directions. The chains in  $\lambda$  are interrupted at the origin, but are continuous in the  $\tau(\mu)$  phase.

The structure factors of the  $\tau(\mu)$  phase for electrons were calculated from the structure model using the *eMap* program (Oleynikov *et al.*, 2005). They are compared quantitatively with the experimental electron diffraction patterns of the  $\tau(\mu)$  phase taken along the  $[001]$ ,  $[010]$  and  $[211]$  axes (Figs. 7*a*, *c* and *e*). The negatives of the ED patterns were digitized using

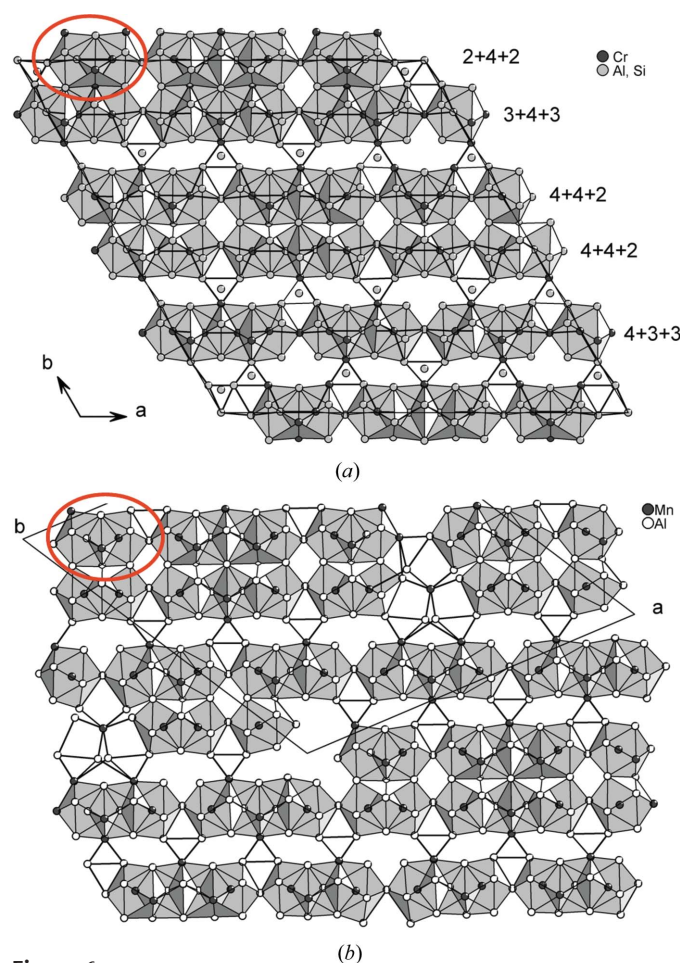


**Figure 6** Comparison of the structures of (a)  $\tau(\mu)$  and (b)  $\lambda$  phases. Both can be described by chains of interpenetrating icosahedra. (a) In  $\tau(\mu)$  there are five such parallel chains continuously running along the  $\langle 100 \rangle$  directions, with the sequences  $2 + 4 + 2$ ,  $3 + 4 + 3$ ,  $4 + 4 + 2$ ,  $4 + 4 + 2$  and  $4 + 3 + 3$ , respectively. (b) In  $\lambda$  the chains are rotated by  $27^\circ$  with respect to the  $\langle 100 \rangle$  directions. The chains are interrupted at the origin. The corresponding icosahedral pairs for  $\tau(\mu)$  and  $\lambda$  are marked by red circles.

an Agfa SnapScan 1200 scanner with a sampling of 300 d.p.i. Intensities of the ED patterns were extracted using a curve-fitting procedure by the program *ELD* (Zou *et al.*, 1993). The

intensities of reflections up to 1.5 Å resolution were merged for each ED pattern according to the space group  $P6_3/mmc$  using the program *Triple* (Calidris, 2000). The number of

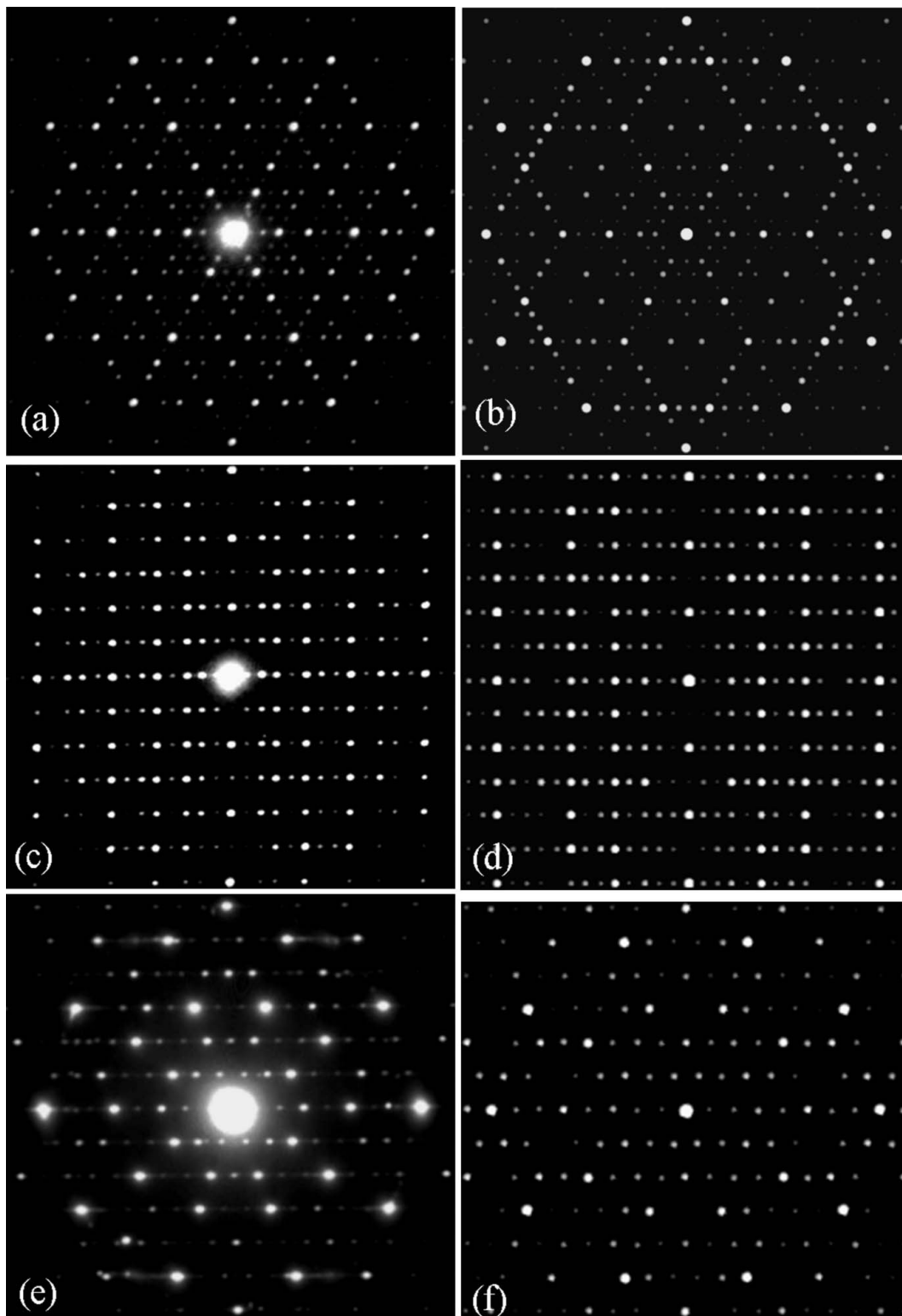


**Figure 7**  
Experimental electron diffraction patterns of  $\tau(\mu)$  taken along the (a) [001], (c) [010] and (e) [211] zone axes on a Philips CM12 transmission electron microscope at 100 kV are compared with those simulated from the structure model using the program *MacTempas*, shown in (b), (d) and (f), respectively. The specimen thicknesses used in the simulations were 100, 50 and 50 Å for (b), (d) and (f).

unique reflections for the [001], [010] and [211] zone axes was 100, 132 and 73, respectively. Within each negative, the  $R_{\text{sym}}$  value was less than 0.085. The  $R(F)$  values compared with the calculated structure factors were 0.334, 0.312 and 0.408 for reflections taken along the [001], [010] and [211] zone axes, respectively. We noticed that intensities of the strongest reflections were very much underestimated, owing to the heavy saturation of these reflections on the negatives. The curve fitting procedure was not enough to recover these heavily saturated reflections. The actual  $R(F)$  value would have been better than those given if the saturated reflections had been correctly estimated. Simulated electron diffraction patterns from the structure model of  $\tau(\mu)$  are shown in Figs. 7(b), (d) and (f). They correspond quite well with the experimental electron-diffraction patterns in Figs. 7(a), (c) and (e). Thus, the structure model deduced for  $\tau(\mu)$  from  $\lambda$  can be taken as a good preliminary model, suitable for structure refinement with X-ray or electron diffraction data.

## 6. Conclusions

Two closely related quasicrystal approximants are expected to have similar crystallographic structure-factor amplitudes and phases for the strong reflections. The structure factors can be transformed from a known approximant to those of an unknown approximant according to their relations in reciprocal space. A structure model can be obtained by Fourier transformation of these structure factors. This strong-reflections approach is a general method for solving unknown quasicrystal approximants from a related known quasicrystal approximant.

## References

- Calidris (2000). *Triple* manual. Manhemsvägen 4, SE-106 91 Sollentuna, Sweden. <http://www.calidris-em.com>.
- Christensen, J., Oleynikov, P., Hovmöller, S. & Zou, X. D. (2004). *Ferroelectrics*, **305**, 273–277.
- Gjønnnes, J., Hansen, V., Berg, B. S., Runde, P., Cheng, Y. F., Gjønnnes, K., Dorset, D. L. & Gilmore, C. J. (1998). *Acta Cryst. A* **54**, 306–319.
- He, Z. B. & Kuo, K. H. (2004). *J. Alloys Compds.* **373**, 39–47.
- Kreiner, G. & Franzen, H. F. (1997). *J. Alloys Compds.* **261**, 83–104.
- Li, X. Z., Hiraga, K. & Yamamoto, A. (1997). *Philos. Mag. A*, **76**, 657–666.
- Marsh, R. E. (1998). *Acta Cryst. B* **54**, 925–926.
- Mo, Z. M., Sui, H. X., Ma, X. L. & Kuo, K. H. (1998). *Metall. Mater. Trans. A*, **29**, 1565–1571.
- Mo, Z. M., Zhou, H. Y. & Kuo, K. H. (2000). *Acta Cryst. B* **56**, 392–401.
- Oleynikov, P., Hovmöller, S. & Zou, X. D. (2005). In preparation.
- Robinson, K. (1952). *Acta Cryst.* **5**, 397–403.
- Shechtman, D., Blech, I., Gratias, D. & Cahn, J. W. (1984). *Phys. Rev. Lett.* **53**, 1951–1953.
- Shoemaker, C. B., Keszler, D. A. & Shoemaker, D. P. (1989). *Acta Cryst. B* **45**, 13–20.
- Silva, W. P. & Silva, C. M. D. P. S. (2005). *Lab Fit Curve Fitting Software* (Nonlinear Regression and Treatment of Data Program), Version 7.2.31. Universidade Federal de Campina Grande, Brazil.
- Taylor, M. A. (1959). *Acta Cryst.* **12**, 393–396.
- Weirich, T. E., Ramlau, R., Simon, A., Hovmöller, S. & Zou, X. D. (1996). *Nature (London)*, **382**, 144–146.
- Weirich, T. E., Zou, X. D., Ramlau, R., Simon, A., Cascarano, G. L., Giacomazzo, C. & Hovmöller, S. (2000). *Acta Cryst. A* **56**, 29–35.
- Yvon, K., Jeitschko, W. & Parthé, E. J. (1977). *J. Appl. Cryst.* **10**, 73–74.
- Zhang, H., Oleynikov, P., Hovmöller, S. & Zou, X. D. (2006). *Philos. Mag.* In the press.
- Zou, X. D., Sukharev, Y. & Hovmöller, S. (1993). *Ultramicroscopy*, **52**, 436–444.
- Zou, X. D., Mo, Z. M., Hovmöller, S., Li, X. Z. & Kuo, K. H. (2003). *Acta Cryst. A* **59**, 526–539.